Research Article

SCISET
www.sciset.com

Research Chronicle in Health Sciences

2022
Vol. 8 No. 1: 101

Multiscale Visualization of Gold Nanoparticle Uptake in HPV-Related Cervical Lesions Using Surface-Enhanced Raman Spectroscopy

Cardo Miota[1]*, Hernandez Rincon[2], Jones Nunez[3]

[1]Department of Psychiatry and Biobehavioral Sciences, David Geffen School of Medicine, UCLA, Los Angeles, CA, USA
2Institute, NewYork-Presbyterian Hospital, Irving Institute for Clinical and Translational Research, New York, NY, USA
3Psychiatry and Biobehavioral Sciences, David Geffen School of Medicine, UCLA, Los Angeles, CA, USA

Corresponding author:
Cardo Miota, Department of Psychiatry and Biobehavioral Sciences, David Geffen School of Medicine, UCLA, Los Angeles, CA, USA,
E-mail: cardo.m@mednet.ucla.edu

Received: March 06, 2022; **Accepted:** March 28, 2022; **Published:** April 10, 2022

Citation: Miota C, et al. Multiscale Visualization of Gold Nanoparticle Uptake in HPV-Related Cervical Lesions Using Surface-Enhanced Raman Spectroscopy. Research Chronicle in Health Sciences. Vol. 8 No. 1: 101

Abstract

Gold nanoparticles (AuNPs) were synthesized using the Turkevich reduction approach and employed to investigate their interactions with human papillomavirus (HPV)-infected and malignant cervical tissues. A combination of scanning electron microscopy (SEM), energy-dispersive X-ray spectroscopy (EDS), confocal microscopy, multiphoton microscopy, and surface-enhanced Raman spectroscopy (SERS) was utilized to characterize nanoparticle localization and tissue-specific responses. SEM and EDS analyses verified the successful incorporation and distribution of AuNPs within both HPV-positive and cancerous cervical specimens. Optical characterization revealed a prominent plasmonic absorption peak at approximately 520 nm. Furthermore, excitation at 900 nm enabled two-photon fluorescence imaging in the red spectral region, providing detailed visualization of tissue architecture and nanoparticle distribution. An additional infrared absorption feature was observed, likely resulting from nanoparticle aggregation within the tissue matrix. To explore molecular-level alterations, SERS measurements were performed on AuNP-treated samples, generating an average of 1,000 spectra per tissue type. Comparative spectral analysis demonstrated distinct differences between HPV-infected and malignant cervical tissues, particularly in Raman bands associated with nucleic acid components. These findings suggest that AuNP-enhanced SERS, combined with advanced optical imaging techniques, may offer a rapid and sensitive platform for the detection and discrimination of cervical cancer-related pathological changes.

Key words: Gold nanoparticles; Human papillomavirus (HPV); Cervical malignancy; Surface-enhanced Raman spectroscopy; Two-photon microscopy; Confocal imaging; Multiphoton microscopy; Optical diagnostics.

Introduction

Cervical cancer remains a major public health challenge and is among the most frequently diagnosed malignancies affecting women worldwide. According to estimates from the World Health Organization, approximately 530,000 new cases were reported in 2012, making cervical cancer the fourth most common cancer in women globally. During the same period, the disease accounted for nearly 7.5% of cancer-related deaths among women. The burden of cervical cancer can be considerably reduced through timely detection of precancerous lesions, particularly cervical intraepithelial neoplasia (CIN), before progression to invasive disease [1]. Persistent infection with high-risk human papillomavirus (HPV) strains, especially HPV-16 and HPV-18, has been recognized as the principal etiological factor driving the development of cervical dysplasia and carcinoma [2,3].

Screening strategies have significantly contributed to reducing cervical cancer incidence and mortality. Among these, the Papanicolaou (Pap) smear remains the most widely adopted

diagnostic approach. Although the method demonstrates high specificity, often ranging between 95% and 98%, its sensitivity is comparatively limited, with reported values close to 50% [4]. To overcome this limitation and reduce false-negative outcomes, complementary approaches such as HPV DNA testing and automated cytological assessment have been incorporated into screening programs [5-7]. In cases where abnormal cytological findings are detected, additional diagnostic procedures including colposcopy, histopathological examination, and tissue biopsy are typically required. However, interpretation of these assessments frequently depends on subjective evaluation by clinicians and pathologists, which may contribute to diagnostic variability. Furthermore, subtle premalignant alterations are not always visually apparent during conventional examination.

The demand for more accurate and objective diagnostic methodologies has stimulated interest in optical and spectroscopic techniques capable of probing biochemical alterations at the molecular level. Among these technologies, Raman spectroscopy has emerged as a promising analytical tool for cancer detection and characterization. Numerous studies have demonstrated its applicability in identifying molecular signatures associated with breast, prostate, esophageal, colorectal, lung, oral, and cervical cancers [8-14]. The microscopic implementation of Raman spectroscopy enables detailed examination of intracellular structures, including nuclei, nucleoli, chromatin organization, and other cellular components [10,15]. Owing to its high spatial resolution and molecular specificity, the technique can also detect individual biomolecular constituents such as adenine, tyrosine, and phenylalanine, providing valuable biochemical information about tissue pathology [16-18].

The analytical performance of Raman spectroscopy can be substantially enhanced through Surface-Enhanced Raman Scattering (SERS), a technique capable of amplifying Raman signals by several orders of magnitude while preserving molecular specificity [19-21]. SERS relies on the interaction between analyte molecules and plasmonic nanostructures, typically composed of noble metals such as gold or silver. Excitation of localized surface plasmon resonances generates strong electromagnetic fields near the nanoparticle surface, producing significant signal enhancement [16,22-24]. Such enhancement is most effective when target molecules are located within a short distance of the nanostructured substrate, generally less than 100 nm from the metallic surface.

Gold nanoparticles (AuNPs) have attracted considerable attention in biomedical research because of their excellent biocompatibility and tunable optical properties. By controlling nanoparticle size, shape, and morphology, the plasmon resonance wavelength can be adjusted across the visible and near-infrared spectral regions. This tunability is particularly advantageous for biological applications because near-infrared light exhibits minimal absorption by tissue, facilitating deeper optical penetration and improved diagnostic performance [25]. Beyond SERS applications, AuNPs can also enhance other optical imaging modalities, including two-photon imaging (TPI). TPI is a non-invasive imaging technique that employs near-infrared excitation to achieve high-resolution visualization at penetration depths extending hundreds of micrometers into biological tissues [26-28].

Previous investigations have demonstrated that plasmonic nanostructures can generate enhanced two-photon signals through resonant coupling between incident light and surface plasmon resonances, resulting in localized electromagnetic field amplification [26,29,30]. While conventional TPI commonly relies on organic fluorophores as contrast agents [31], recent advances have expanded the range of imaging probes to include quantum dots [32], metallic nanoparticles [33-36], and gold nanorods [37,38]. These developments highlight the growing potential of plasmonic nanomaterials for integrated imaging and sensing applications.

In the present study, the interactions between gold nanoparticles and HPV-infected as well as malignant cervical tissues were systematically investigated. A multimodal characterization strategy incorporating scanning electron microscopy (SEM), confocal microscopy, chemical mapping, and two-photon imaging was employed to evaluate nanoparticle distribution and tissue morphology. The results revealed nanoparticle aggregation within the tissue microenvironment, generating localized electromagnetic field enhancement that facilitated both SERS measurements and two-photon emission in the red spectral region under 900 nm excitation. These preliminary findings demonstrate distinct molecular and structural differences between HPV-associated and cancerous cervical tissues, suggesting that AuNPs may serve as valuable optical probes for future diagnostic, sensing, and cancer-screening applications.

Materials and Methods

Synthesis of Gold Nanoparticles

Gold nanoparticles (AuNPs) were synthesized following a modified Turkevich citrate-reduction protocol [39]. Initially, a 0.1 M chloroauric acid solution was prepared by dissolving 0.5 g of $HAuCl_4$ (99.999%, Sigma-Aldrich) in 14.715 mL of deionized water. Separately, a 1% (w/v) sodium citrate solution was obtained by dissolving 0.0375 g of $Na_3C_6H_5O_7$ (Sigma-Aldrich) in 3.75 mL of deionized water (Table 1).

Table 1: Experimental conditions and analytical techniques used in the study.

Parameter	Description
Nanoparticle synthesis method	Modified Turkevich citrate reduction method
Gold precursor	$HAuCl_4$ (0.1 M)

Reducing/Stabilizing agent	Sodium citrate (1% w/v)
Average AuNP size	13 ± 2 nm
Surface plasmon resonance peak	520 nm
Tissue type	HPV-infected and cervical cancer tissues
Tissue preservation	Formalin-fixed paraffin-preserved (FFPP)
Tissue section thickness	5 µm
AuNP incubation temperature	37°C
AuNP incubation time	2 h
SEM analysis	JEOL JSM-7800F
EDS analysis	Oxford Instruments EDS system
TEM analysis	FEI Titan 80–300
Confocal excitation wavelength	543 nm
Two-photon excitation wavelength	900 nm
Raman excitation wavelength	785 nm
Raman spectral range	700–1700 cm^{-1}
Raman integration time	20 s
Number of mapped regions/ samples	≥10
Storage temperature of AuNPs	4°C

For nanoparticle synthesis, 250 µL of the $HAuCl_4$ solution and 3.75 mL of the sodium citrate solution were introduced into 25 mL of boiling deionized water under continuous magnetic stirring at 400 rpm. The reaction mixture gradually developed a characteristic ruby-red coloration, indicating the formation of AuNPs. The colloidal suspension was subsequently allowed to cool to room temperature and filtered to remove any large aggregates. The resulting nanoparticle dispersion was stored at 4°C until further use.

Preparation of Cervical Tissue Samples

Formalin-fixed paraffin-preserved (FFPP) cervical tissue specimens were obtained through the Pathology Department of the Instituto de Seguridad y Servicios Sociales de los Trabajadores del Estado (ISSSTE), Guanajuato, Mexico. Tissue evaluation and classification were performed by an experienced pathologist. Fifteen samples representing different grades of cervical intraepithelial neoplasia (CIN) were selected for analysis. Five specimens corresponded to CIN1 (low-grade squamous intraepithelial lesions), five to CIN2 (moderate-grade lesions), and five to CIN3 (high-grade lesions). Each specimen represented an independent patient case (Table 2) [40].

For histopathological assessment, tissue sections were initially dewaxed using xylene (KARAL) and absolute ethanol (KEM). For nanoparticle studies, two parallel FFPP sections of 5 µm thickness were obtained from each paraffin block using a microtome. The sections were mounted on glass microscope slides and allowed to dry prior to further processing.

Tissue Deparaffinization and Rehydration

Prior to nanoparticle treatment, mounted tissue sections were incubated at 60°C for 1 h to soften the paraffin matrix. Deparaffinization was carried out by immersing the slides twice in xylene for 15 min per treatment. Subsequently, tissues were rehydrated through a graded ethanol series consisting of 100%, 90%, 70%, and 30% ethanol, each for 10 min. Following rehydration, the samples were immersed in phosphate-buffered saline (PBS, 1×) for 5 min and rinsed with distilled water for an additional 5 min.

Gold Nanoparticle Impregnation

Following rehydration, excess surface moisture was removed from the tissue sections. A hydrophobic boundary was then drawn around each specimen using Pappen® ink to confine the nanoparticle suspension to the tissue region and prevent spreading across the slide.

The prepared samples were placed on a heating platform and incubated with the AuNP colloidal solution at 37°C for 2 h. During incubation, tissue hydration was monitored continuously, and additional colloidal solution was supplied when necessary to prevent drying. Upon completion of the incubation period, samples were gently rinsed with distilled water to remove excess nanoparticles.

Table 2: Summary of imaging and spectroscopic findings in HPV-infected and malignant cervical tissues.

Analytical Method	HPV-Infected Tissue	Malignant Cervical Tissue	Key Observation
SEM	Relatively preserved cellular morphology	Enlarged and irregular nuclei	Nuclear enlargement up to 300%
EDS	Presence of AuNPs in tissue	Higher AuNP accumulation in nuclei	Preferential nuclear localization
Confocal Microscopy	Moderate fluorescence signal	Enhanced signal intensity	Effective AuNP uptake
Two-Photon Imaging	Tissue morphology visible	More pronounced structural alterations	Red-region emission under 900 nm excitation
SERS Analysis	Distinct DNA-related Raman bands	Altered DNA spectral signatures	Molecular differences detected
Raman Intensity	Lower enhancement	Greater enhancement in some regions	AuNP aggregation promotes local field enhancement
Tissue Architecture	Less disrupted organization	Significant morphological changes	Disease progression evident
Diagnostic Potential	Detection of HPV-associated changes	Identification of cancer-associated changes	Potential rapid screening approach

For confocal and multiphoton imaging experiments, several drops of DABCO (1,4-diazabicyclo[2.2.2]octane) mounting medium were applied before placing a coverslip over the specimen. Care was taken to avoid air-bubble formation. For Raman spectroscopic analysis, DABCO was omitted following a previously reported protocol for preserving biological samples intended for chemical characterization [41]. Instead, the tissues were dried at 90°C for 3 min prior to spectral acquisition.

Characterization Techniques

Electron Microscopy and Elemental Analysis

The morphology and size distribution of the synthesized AuNPs were evaluated using transmission electron microscopy (TEM). Measurements were performed with a FEI Titan 80–300 microscope operating at an accelerating voltage of 300 kV.

Tissue morphology and nanoparticle localization were examined using a JEOL JSM-7800F scanning electron microscope (SEM). Elemental composition and spatial distribution of gold within the tissue sections were further investigated using energy-dispersive X-ray spectroscopy (EDS) integrated with an Oxford Instruments analytical system.

Optical Spectroscopy and Microscopy

Optical absorption characteristics of the AuNP colloidal suspension were determined using a PerkinElmer Lambda 900 UV–Vis spectrophotometer with a spectral resolution of 2 nm.

Confocal and multiphoton imaging experiments were conducted using a Zeiss LSM-710-NLO laser scanning microscope equipped with a Chameleon Vision II ultrafast laser system (Coherent, USA). The laser source provided tunable excitation wavelengths ranging from 680 to 1040 nm with pulse durations of approximately 140 fs and a repetition rate of 80 MHz. Confocal fluorescence images were acquired using 543 nm excitation, whereas two-photon imaging was performed at an excitation wavelength of 900 nm.

Raman Spectroscopic Analysis

Raman measurements were carried out using a Renishaw inVia Raman microscope equipped with a 20× objective lens. Spectra were collected using a 785 nm excitation laser with an output power of approximately 5 mW at the sample surface. Each spectrum was recorded with an integration time of 20 s over the spectral region extending from 700 to 1700 cm^{-1}.

To ensure representative sampling, Raman mapping was performed on a minimum of ten independent regions within each tissue specimen, depending on slide quality and tissue integrity. Every selected region was analyzed in duplicate. The reported spectra correspond to the averaged response obtained from all mapped regions within each sample.

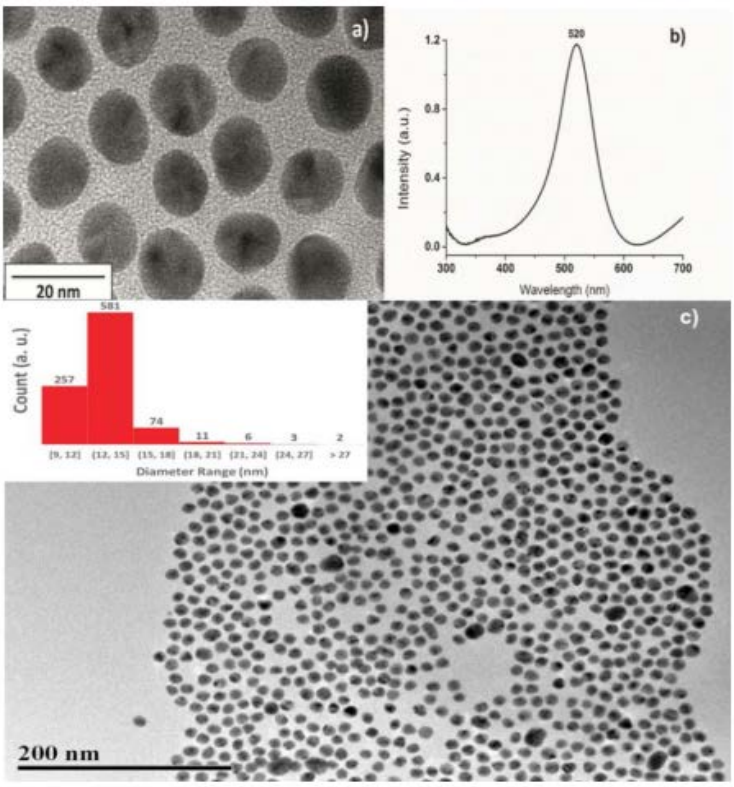

Figure 1: (a) High magnification TEM micrographs of gold nanoparticles; (b) absorption spectra of the gold nanoparticles; (c) TEM micrograph, inset shows the size distribution of gold nanoparticles.

Results and Discussion

Morphological and Optical Characterization of Gold Nanoparticles

The structural characteristics of the synthesized gold nanoparticles were initially examined using transmission electron microscopy (TEM). A representative TEM image is presented in Figure 1a, revealing that the particles exhibit a predominantly quasi-spherical to slightly elongated morphology with good dispersion throughout the sample. The nanoparticles appeared relatively uniform in shape, indicating effective control of particle formation during the citrate-reduction synthesis process.

The optical behavior of the AuNP colloidal suspension was investigated through UV–Vis spectroscopy. As illustrated in Figure 1b, the absorption spectrum displayed a distinct surface plasmon resonance (SPR) band centered at approximately 520 nm. This plasmonic feature is characteristic of citrate-stabilized gold nanoparticles and agrees well with previous reports describing AuNPs synthesized using the Turkevich method [40]. The observed SPR position is also consistent with the ruby-red coloration of the colloidal solution, confirming successful nanoparticle formation and stability.

A lower-magnification TEM image is shown in Figure 1c, providing additional information regarding particle distribution within the sample. The corresponding particle-size histogram, presented in the inset of the figure, demonstrates a relatively narrow size distribution. Statistical analysis indicated an average nanoparticle diameter of approximately 13 ± 2 nm. The limited variation in particle size suggests a homogeneous synthesis process, which is advantageous for obtaining reproducible optical properties and reliable plasmonic enhancement effects during subsequent imaging and SERS investigations.

The combination of TEM and UV–Vis results confirm the successful synthesis of well-dispersed gold nanoparticles with dimensions suitable for plasmonic-based biomedical applications. The observed size range and SPR characteristics are expected to facilitate efficient interaction with biological tissues and contribute to the electromagnetic field enhancement required for both Raman signal amplification and optical imaging studies.

Conclusion

This study investigated the interaction of gold nanoparticles (AuNPs) with HPV-infected and malignant cervical tissues using electron microscopy, optical imaging, and surface-enhanced Raman spectroscopy (SERS). SEM analysis revealed significant morphological alterations, including nuclear enlargement of up to 300%, indicating cellular transformation associated with disease progression. EDS measurements confirmed the presence and preferential localization of AuNPs within the nuclear region of tissue cells. Multiphoton imaging successfully visualized tissue morphology through red-region emission under 900 nm excitation, demonstrating the suitability of AuNPs as optical contrast agents. Furthermore, the plasmonic properties of the nanoparticles generated strong local electromagnetic field enhancement, enabling sensitive SERS detection of molecular differences between HPV-positive and cancerous tissues. Distinct spectral variations were primarily observed in DNA-related Raman bands, suggesting changes in nuclear composition during carcinogenesis. The combined application of AuNP-assisted imaging and SERS provides a promising approach for rapid tissue characterization and may support the development of sensitive diagnostic tools for cervical cancer detection and monitoring.

References

1. Ferlay J, Soerjomataram I, Dikshit R, Eser S, Mathers C, Rebelo M, et al. Cancer incidence and mortality worldwide: Sources, methods and major patterns in GLOBOCAN 2012. Int J Cancer. 2015;136:E359-E386.
2. Bosch FX, Lorincz A, Muñoz N, Meijer CJLM, Shah KV. The causal relation between human papillomavirus and cervical cancer. J Clin Pathol. 2002;55:244-265.
3. Walboomers JMM, Jacobs MV, Manos MM, Bosch FX, Kummer JA, Shah KV, et al. Human papillomavirus is a necessary cause of invasive cervical cancer worldwide. J Pathol. 1999;189:12-19.
4. Nanda K, McCrory DC, Myers ER, Bastian LA, Hasselblad V, Hickey JD, et al. Accuracy of the Papanicolaou test in screening for and follow-up of cervical cytologic abnormalities. Ann Intern Med. 2000;132:810-819.
5. Cuzick J, Clavel C, Petry KU, Meijer CJLM, Hoyer H, Ratnam S, et al. Overview of the European and North American studies on HPV testing in primary cervical cancer screening. Int J Cancer. 2006;119:1095-1101.
6. Schiffman M, Castle PE. The promise of global cervical-cancer prevention. N Engl J Med. 2005;353:2101-2104.
7. Wright TC Jr, Schiffman M, Solomon D, Cox JT, Garcia F, Goldie S, et al. Interim guidance for the use of human papillomavirus DNA testing. Obstet Gynecol. 2004;103:304-309.
8. Lyng FM, Traynor D, Nguyen TNQ, Meade AD, Barr H, Ramos IRM. Discrimination of normal and malignant cells using Raman spectroscopy. Expert Rev Mol Diagn. 2012;12:169-176.
9. Ramos IRM, Malkin A, Lyng FM. Current advances in the application of Raman spectroscopy for molecular diagnosis of cervical cancer. Biomed Res Int. 2015;2015:561242.
10. Shaikh R, Vikas V, Rao K. Raman spectroscopy for early detection of cervical cancer: A review. Diagnostics. 2023;13:1024.

11. Duraipandian S, Zheng W, Ng J, Huang Z. Simultaneous fingerprint and high-wavenumber Raman spectroscopy for cervical precancer detection. Anal Chem. 2012;84:5913-5919.
12. Duraipandian S, Traynor D, Kearney P, Martin C, Lyng FM. Raman spectroscopic detection of high-grade cervical cytology using morphologically normal cells. Sci Rep. 2018;8:15048.
13. Barik AK, Prabhakar N, Singh GP, et al. Micro-Raman spectroscopy study of normal and abnormal cervical smears. Gynecol Oncol. 1997;66:59-65.
14. Raja P, Aruna P, Koteeswaran D, et al. Characterization of blood plasma of normal and cervical cancer patients using NIR Raman spectroscopy. Vib Spectrosc. 2019;102:1-7.
15. Huang Z, McWilliams A, Lui H, McLean DI, Lam S, Zeng H. Near-infrared Raman spectroscopy for optical diagnosis of epithelial precancer. Int J Cancer. 2003;107:1047-1052.
16. Kneipp K, Kneipp H, Itzkan I, Dasari RR, Feld MS. Surface-enhanced Raman scattering and biophysics. J Phys Condens Matter. 2002;14:R597-R624.
17. Moskovits M. Surface-enhanced Raman spectroscopy: A brief retrospective. J Raman Spectrosc. 2005;36:485-496.
18. Camden JP, Dieringer JA, Wang Y, Masiello DJ, Marks LD, Schatz GC, et al. Probing the structure of single-molecule SERS hot spots. J Am Chem Soc. 2008;130:12616-12617.
19. Nie S, Emory SR. Probing single molecules and single nanoparticles by surface-enhanced Raman scattering. Science. 1997;275:1102-1106.
20. Le Ru EC, Etchegoin PG. Principles of Surface-Enhanced Raman Spectroscopy. Amsterdam: Elsevier; 2009.
21. Aroca R. Surface-Enhanced Vibrational Spectroscopy. Chichester: Wiley; 2006.
22. Otto A. The chemical and electromagnetic mechanisms of SERS. J Raman Spectrosc. 2005;36:497-509.
23. Schatz GC, Van Duyne RP. Electromagnetic mechanism of SERS. In: Surface-Enhanced Raman Scattering. Berlin: Springer; 2006. p. 19-45.
24. Stiles PL, Dieringer JA, Shah NC, Van Duyne RP. Surface-enhanced Raman spectroscopy. Annu Rev Anal Chem. 2008;1:601-626.
25. Jain PK, Huang X, El-Sayed IH, El-Sayed MA. Noble metals on the nanoscale: Optical and photothermal properties. Acc Chem Res. 2008;41:1578-1586.
26. El-Sayed IH, Huang X, El-Sayed MA. Surface plasmon resonance scattering and absorption of anti-EGFR antibody conjugated gold nanoparticles. Nano Lett. 2005;5:829-834.
27. Huang X, Jain PK, El-Sayed IH, El-Sayed MA. Gold nanoparticles: Interesting optical properties and biomedical applications. Nanomedicine. 2007;2:681-693.
28. Denk W, Strickler JH, Webb WW. Two-photon laser scanning fluorescence microscopy. Science. 1990;248:73-76.
29. So PT, Dong CY, Masters BR, Berland KM. Two-photon excitation fluorescence microscopy. Annu Rev Biomed Eng. 2000;2:399-429.
30. Helmchen F, Denk W. Deep tissue two-photon microscopy. Nat Methods. 2005;2:932-940.
31. Zipfel WR, Williams RM, Webb WW. Nonlinear magic: Multiphoton microscopy in the biosciences. Nat Biotechnol. 2003;21:1369-1377.
32. Larson DR, Zipfel WR, Williams RM, Clark SW, Bruchez MP, Wise FW, et al. Water-soluble quantum dots for multiphoton fluorescence imaging. Science. 2003;300:1434-1436.
33. Mohamed MB, Volkov V, Link S, El-Sayed MA. The lightning gold nanorods: Fluorescence enhancement and applications. Chem Phys Lett. 2000;317:517-523.
34. Durr NJ, Larson T, Smith DK, Korgel BA, Sokolov K, Ben-Yakar A. Two-photon luminescence imaging of cancer cells using gold nanorods. Nano Lett. 2007;7:941-945.
35. Tong L, Zhao Y, Huff TB, Hansen MN, Wei A, Cheng JX. Gold nanorods mediate imaging and therapy. Adv Mater. 2007;19:3136-3141.
36. Wang H, Huff TB, Zweifel DA, He W, Low PS, Wei A, et al. In vitro and in vivo two-photon luminescence imaging with gold nanorods. Proc Natl Acad Sci USA. 2005;102:15752-15756.
37. Boyer D, Tamarat P, Maali A, Lounis B, Orrit M. Photothermal imaging of nanometer-sized metal particles. Science. 2002;297:1160-1163.
38. Cognet L, Tardin C, Boyer D, Choquet D, Tamarat P, Lounis B. Single metallic nanoparticle imaging. Proc Natl Acad Sci USA. 2003;100:11350-11355.
39. Turkevich J, Stevenson PC, Hillier J. A study of the nucleation and growth processes in the synthesis of colloidal gold. Discuss Faraday Soc. 1951;11:55-75.
40. Frens G. Controlled nucleation for the regulation of particle size in monodisperse gold suspensions. Nat Phys Sci. 1973;241:20-22.
41. Ceja-Fdez A, González-Solís JL, Hernández-Arteaga AC, Baldovino-Pantaleón O, Rivera-Márquez JA, Ramírez-Elías MG. Imaging and SERS study of the Au nanoparticles interaction with HPV and carcinogenic cervical tissues. Molecules. 2021;26:3758.